Effect of Solute Size and Solute−Water Attractive Interactions on Hydration Water Structure around Hydrophobic Solutes

Henry S. Ashbaugh[†,‡] and Michael E. Paulaitis*[,§]

Contribution from the Department of Chemical Engineering, Princeton University, Princeton, New Jersey 08544, and Department of Chemical Engineering, The Johns Hopkins University, Baltimore, Maryland 21218

Received May 31, 2001

Abstract: Using Monte Carlo simulations, we investigated the influence of solute size and solute−water attractive interactions on hydration water structure around spherical clusters of 1, 13, 57, 135, and 305 hexagonally close-packed methanes and the single hard-sphere (HS) solute analogues of these clusters. We obtain quantitative results on the density of water molecules in contact with the HS solutes as a function of solute size for HS radii between 3.25 and 16.45 Å. Analysis of these results based on scaled-particle theory yields a hydration free energy/surface area coefficient equal to 139 cal/(mol Å^2), independent of solute size, when this coefficient is defined with respect to the van der Waals surface of the solute. The same coefficient defined with respect to the solvent-accessible surface decreases with decreasing solute size for HS radii less than ∼10 Å. We also find that solute−water attractive interactions play an important role in the hydration of the methane clusters. Water densities in the first hydration shell of the three largest clusters are greater than bulk water density and are insensitive to the cluster size. In contrast, contact water densities for the HS analogues of these clusters decrease with solute size, falling below the bulk density of water for the two largest solutes. Thus, the large HS solutes dewet, while methane clusters of the same size do not.

Introduction

The distinction between molecular hydrophobic effects, quantified by hydrocarbon-to-water transfer free energies, and hydrophobic driving forces that influence self-assembly on larger length scales (e.g., micelle formation and protein folding) was first noted by Tanford.[1] His observation was based on the large discrepancy between the measured water−hydrocarbon interfacial tension and the incremental free energy of hydrophobic hydration per solute surface area obtained from *n*-alkane solubility data. Israelachvili et al.[2] also noted this discrepancy in proposing an elementary theory of surfactant self-assembly in aqueous solution. Adopting the phenomenological approach of linearly correlating free energies of hydrophobic hydration with solute surface areas, they resolved the discrepancy by defining *n*-alkane surface areas with respect to the van der Waals surface, rather than the solvent-accessible surface of these hydrocarbons. Thus, they calculated a hydration free energy/surface area coefficient from *n*-alkane solubility data that was close to the experimental value for the macroscopic water−hydrocarbon interfacial tension.

A more recent example of the distinction between molecular and microscopic hydrophobic interactions is found in measurements of a long-range attractive force between microscopic hydrophobic surfaces, which cannot be explained on the basis of molecular hydrophobic effects.[3,4] The lack of a definitive interpretation of these measurements underscores the need for a quantitative theory of hydrophobic phenomena beyond molecular hydrophobic effects. In general, the need for a unified, quantitative description of both molecular and macroscopic hydrophobic phenomena arises because hydrophobic driving forces play an important role in self-assembly on intermediate-length scales and the fact that quantitative descriptions of these driving forces are derived from molecular solubility data, macroscopic interfacial tension measurements, or interpolations of these quantities.

A conceptual basis for a unified thermodynamic treatment of molecular and macroscopic hydrophobic hydration can be found in scaled-particle theory (SPT),[5] the general formulation of which motivates various solvent-exposed surface area models of the free energy of hydrophobic hydration.[6] In the application of SPT to hydrophobic hydration,[7−9] the free energy of cavity formation in water is computed by integrating the compressive force exerted by water molecules on the surface of this cavity as it grows in size. This compressive force is proportional to the local density of water molecules in contact with the cavity surface, which can be expressed in terms of the bulk liquid density, the oxygen−oxygen radial distribution function, and higher order water correlation functions[10] and, on macroscopic-length scales, yields the work against the vapor−liquid surface tension and the pressure. The density of water molecules at the

† Princeton University.
‡ Present address: Theoretical Chemistry and Molecular Physics, Group T-12, MS B268, Los Alamos National Laboratory, Los Alamos, NM 87545.
§ The Johns Hopkins University.

(1) Tanford, C. *Proc. Natl. Acad. Sci. U.S.A.* **1979**, *76*, 4175.
(2) Israelachvili, J. N.; Mitchell, D. J.; Ninham, B. W. *J. Chem. Soc., Faraday Trans. 2* **1976**, *72*, 1525.
(3) Israelachvili, J. N.; Pashley, R. M. *Nature* **1982**, *300*, 341.
(4) Spalla, O. *Curr. Opin. Colloid Interface Sci.* **2000**, *5*, 5.
(5) Reiss, H.; Frisch, H. L.; Lebowitz, J. L. *J. Chem. Phys.* **1959**, *31*, 369.
(6) Roux, B.; Simonson, T. *Biophys. Chem.* **1999**, *78*, 1.
(7) Pierotti, R. A. *J. Phys. Chem.* **1963**, *67*, 1840.
(8) Stillinger, F. H. *J. Solution Chem.* **1973**, *2*, 141.
(9) Postma, J. P. M.; Berendsen, H. J. C.; Haak, J. R. *Faraday Symp. Chem. Soc.* **1982**, *17*, 55.
(10) Pratt, L. R.; Garde, S.; Hummer, G. In *New Approaches to Problems in Liquid-State Theory*; Caccamo, C., Hansen, J.-P., Stell, G., Eds.; NATO Science Series 529; Kluwer: The Netherlands, 1999; p 407.

10.1021/ja016324k CCC: $20.00
Published on Web 10/03/2001

cavity surface is $\rho G(r)$, where $G(r)$ is the contact water density normalized by the bulk water density, ρ. The key quantity in SPT is this contact water density, $G(r)$.

The cavity-size dependence of $G(r)$ is sensitive to the hydration structure of water molecules around the cavity. For small cavities, the compressive force exerted by the solvent increases with increasing cavity size much faster in water than it does, for example, in normal liquid hydrocarbons, due to strong cohesive forces that arise from water hydrogen bonding. Water contact densities, therefore, increase correspondingly faster with increasing cavity size. Previous simulation results[11,12] show a single, broad maximum in $G(r)$ that is thought to define a crossover in hydration behavior on the molecular scale from small to large cavities. This maximum occurs at a cavity radius less than the distance of closest approach assigned to contact between a water molecule and a methane molecule. Cavity sizes substantially larger than the maximum have not heretofore been explored in simulation studies of hydration behavior.

In the limit of a macroscopic cavity, SPT is constructed to satisfy the following exact condition,[8]

$$\lim_{r\to\infty} \rho G(r) = (P/\rho kT)\rho$$

where P is the pressure, kT is the thermal energy, and ρ is the liquid density of water. At room temperature, $P/\rho kT$ is $\sim 2 \times 10^{-5}$ for saturated liquid water.[13] Thus, the density of water molecules in contact with macroscopically large cavities is exceedingly low. In effect, the hydrated planar interface is in contact with a film of water vapor; i.e., it dewets. This SPT prediction of the dewetting of large cavities—or equivalently, large hard-sphere (HS) solutes—distinguishes macroscopic from molecular hydrophobic hydration behavior. The distinction between macroscopic versus molecular hydrophobic hydration in terms of the HS solute size is, however, still an open question.

The modified $G(r)$ expression in Stillinger's application of SPT to water[8] accounts for the effect of strong, directional hydrogen-bonding forces on water structure, which leads to different orientational preferences for water molecules in contact with molecular versus macroscopic cavities. Differences in water orientations near a flat hydrophobic surface compared to small hydrophobic solutes have been observed in molecular simulation studies[14] and, more recently, in surface-specific vibrational spectroscopy experiments.[15] The solute size dependence of these orientational preferences has been examined in molecular simulations of the hydration of repulsive Lennard-Jones (LJ) solutes.[16] It was found that the entropy penalty per water molecule in the first hydration shell associated with solute−water orientational correlations exhibits a maximum at an effective solute diameter of 4 Å. The finding suggests that the loss of water hydrogen bonds, which leads to dewetting of the purely repulsive interface, is a gradual process that actually begins for repulsive LJ solutes only slightly larger in size than methane. Conversely, abrupt dewetting of the surfaces between two repulsive oblate ellipsoids has been observed in molecular simulations as these surfaces are brought to within two water molecular layers of one another.[17] A quantitative explanation for this dewetting behavior has been proposed based on a theory of inhomogeneous fluids.[18]

Dewetting in the SPT analysis of hydrophobic hydration is associated with two factors: the absence of solute−water attractive interactions, the impact of which increases with increasing solute size, and low water vapor densities along the vapor−liquid saturation curve at ambient temperature. Pratt and Chandler[19] considered the influence of solute−water attractive interactions on the density of water molecules in contact with a LJ solute the size of methane and found that these interactions increased the contact density by ~10%. Hummer and Garde[20] extended the Pratt−Chandler analysis to examine the solute size dependence of dewetting LJ solutes in water. An effective cavity expulsion potential was defined as a contribution to the solute−water oxygen potential of mean force and calculated from extensive molecular simulations for LJ solutes up to 7.5 Å in diameter. Cavity expulsion accounts for the loss of favorable water−water interactions (e.g., water hydrogen bonds) as a water molecule approaches the cavity. The loss of hydrogen-bonding interactions is negligible for small cavities, since these hydrogen bonds can be maintained even if the cavity and the test water molecule overlap completely, but this loss becomes progressively more important with increasing cavity size. Hummer and Garde found the cavity expulsion potential to be short-ranged, acting only over the length scale of an individual water molecule. They also showed that solute−water attractive interactions offset cavity expulsion, thus implicating solute−water attractive interactions as a key determinant in the dewetting behavior of hydrophobic solutes. Lee and Rossky[21] likewise found such attractive interactions to be important in their molecular simulations of the hydration of a perfectly flat hydrophobic surface compared to one consisting of hexagonally close-packed LJ spheres approximating methane molecules. Specifically, they observed a pronounced increase in wetting for the molecularly detailed surface, which they attributed to a locally higher attractive potential between a water molecule and the LJ molecules comprising the surface. Wallqvist et al.[22] have shown, however, that these effects are attenuated for hydrophobic surfaces with large negative curvature, i.e., for water confined within spherical cavities 20−24 Å in radius embedded in a hydrophobic continuum. Water density profiles observed in Gibbs ensemble simulations of liquid water within spherical cavities 6−15 Å in radius[23] indicate large enhancements in the contact density relative to bulk water density once attractive LJ interactions between water molecules and the cavity surface exceed a certain critical value.

In this paper, we compare the hydration of discrete spherical clusters of 1, 13, 57, 135, and 305 hexagonally close-packed methanes to the hydration of a single HS solute that is equivalent in size to each of these clusters. These HS solutes have radii of 3.25, 6.55, 9.85, 13.15, and 16.45 Å, respectively, where the radius is defined by the spherical volume inaccessible to the center of the water oxygens. Our results allow us to draw conclusions about the solute size dependence of the hydration water structure around these nonpolar solutes for a range of

(11) Pratt, L. R.; Pohorille, A. *Proc. Natl. Acad. Sci. U.S.A.* **1992**, *89*, 2995.
(12) Pohorille, A.; Pratt, L. R. *J. Am. Chem. Soc.* **1990**, *112*, 5066.
(13) Sandler, S. I. *Chemical and Engineering Thermodynamics*, 3rd ed.; Johns Wiley & Sons: New York, 1999.
(14) Lee, C. Y.; McCammon, J. A.; Rossky, P. J. *J. Chem. Phys.* **1984**, *80*, 4448.
(15) Scatena, L. F.; Brown, M. G.; Richmond, G. L. *Science* **2001**, *292*, 908.
(16) Lazaridis, T.; Paulaitis, M. E. *J. Phys. Chem.* **1994**, *98*, 635.
(17) Wallqvist, A.; Berne, B. J. *J. Phys. Chem.* **1995**, *99*, 2893.
(18) Lum, K.; Chandler, D.; Weeks, J. D. *J. Phys. Chem. B* **1999**, *103*, 4570.
(19) Pratt, L. R.; Chandler, D. *J. Chem. Phys.* **1980**, *73*, 3434.
(20) Hummer, G.; Garde, S. *Phys. Rev. Lett.* **1998**, *80*, 4193.
(21) Lee, C. H.; Rossky, P. J. *J. Chem. Phys.* **1994**, *100*, 3334.
(22) Wallqvist, A.; Gallicchio, E.; Levy, R. M. *J. Phys. Chem.* **2001**, *105*, 6745.
(23) Brovchenko, I.; Paschek, D.; Geiger, A. *J. Chem. Phys.* **2000**, *113*, 5026.

Table 1. Simulation Conditions

solute	N_{water}	L (Å)	N_{passes}
discrete clusters (no. of methanes)			
1	215	18.64	1×10^6
13	550	25.86	3×10^5
57	1200	34.09	1.5×10^5
135	1704	39.00	1×10^5
305	3324	49.00	5×10^4
hard-sphere solutes (sphere radii, Å)			
3.25	215	18.64	1×10^6
6.55	550	25.96	3×10^5
9.85	1435	36.10	1.5×10^5
13.15	2222	42.40	1×10^5
16.45	3670	50.50	5×10^4

sizes from a single methane-sized solute to a solute roughly equivalent in size to a simple micelle or small globular protein. The influence of solute−water attractive interactions on water structure is also examined by comparing the hydration of the methane clusters to their HS analogues.

Computational Methods

Canonical ensemble Monte Carlo simulations were carried out for a single solute consisting of a cluster of methane molecules or a comparably sized, single HS solute in a bath of water molecules at 25 °C. Water−water pair interactions were modeled using the simple point charge (SPC) potential.[24] The distance between neighboring methanes within each cluster was fixed at 4.19 Å, which corresponds to the minimum in the OPLS LJ united atom methane−methane pair potential.[25] LJ parameters for the methane−water pair potential were determined from Lorenz−Berthelot combining rules. All LJ interactions were truncated at half the simulation box length. Long-range electrostatic interactions were evaluated using Ewald summation. The number of water molecules in each simulation was chosen to give an average water density of 0.997 g/cm^3 ±0.5% in the corners of the simulation box (i.e., outside a sphere of radius half the box length, centered on the solute). The number of water molecules, box size, and number of Monte Carlo passes (one pass = one attempted move on every water molecule in the simulation) used in each simulation are listed in Table 1. From the isothermal compressibility of SPC water at 25 °C ($\rho^{sat}kT\chi_T = 0.062$), pressure fluctuations during the simulations are estimated to be on the order of ±100 bar and, as such, have a negligible effect on the thermodynamics of hydrophobic hydration.

Results and Discussion

The HS solute−water oxygen radial distribution functions (RDFs) obtained from simulation are plotted in Figure 1. The simulation value of $G(r)$ for each solute is shown as an open circle. These values are fit to the functional form for $G(r)$ proposed by Stillinger[8] that interpolates between the known molecular and macroscopic limits,

$$G(r) = \begin{cases} \dfrac{1 + (\pi\rho/r)\int_0^{2r} g_{ww}(r')(r'^3 - 2rr'^2)\,dr'}{1 - 4\pi\rho r^3/3 + (\pi\rho)^2\int_0^{2r} g_{ww}(r')(r'^5/6 - 2r^2r'^3 + 8r^3r'^2/3)\,dr'} & r < 1.95\ \text{Å} \\ P/\rho kT + 2\gamma_\infty/\rho kTr + G_2/r^2 + G_4/r^4 & r > 1.95\ \text{Å} \end{cases} \quad (1)$$

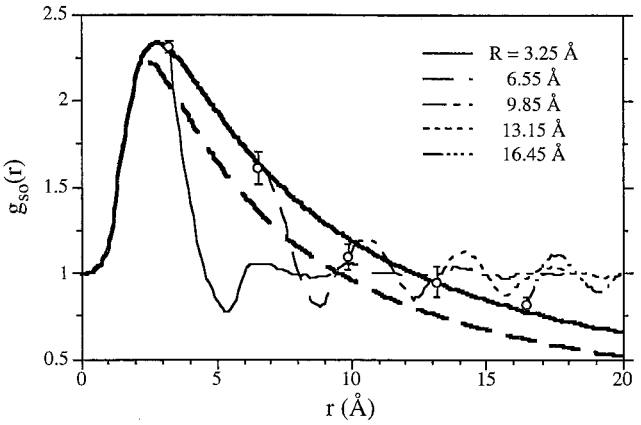

Figure 1. HS solute−SPC water oxygen radial distribution functions and contact values of the radial distribution function for the HS radii indicated in the legend. $G(r)$, the contact value of the RDF, for each solute (open circles) obtained from simulation is compared to $G(r)$ calculated using eq 1 with $\gamma = 139$ and 108 cal/(mol Å^2) (heavy solid and dashed lines, respectively). The errors bars denote one standard deviation in the simulation values of $G(r)$.

where g_{ww} is the oxygen−oxygen radial distribution function for water and γ_∞ is the surface tension in the limit of a planar interface (i.e., as $r \rightarrow \infty$), which is typically taken to be the vapor−liquid interfacial tension of water. We use γ_∞ as an adjustable parameter in this fit and neglect the term $P/\rho kT$, which is on the order of 10^{-5} at room temperature. Including this term has little effect on $G(r)$. The constants G_2 and G_4 are chosen to match $G(r)$ and its first derivative at $r = 1.95$ Å, the separation at which triplet and higher-order water correlations begin to make significant contributions to $G(r)$. This separation is well below the maximum in $G(r)$ at $r \sim 2.8$ Å, which in turn is less than the radius corresponding to the exclusion volume for the smallest (methane-sized) HS solute studied. For larger HS solutes, the simulation values of $G(r)$ in Figure 1 decrease smoothly with increasing solute size, such that the contact density falls below the density of bulk water for the two largest solutes. The contact density for the largest HS solute is, however, still much greater than $\sim 2 \times 10^{-5}$, the SPT value for a macroscopic cavity. Equation 1 accurately captures this solute size dependence with $\gamma_\infty = 139$ cal/(mol Å^2). Using the vapor−liquid interfacial tension of SPC/E water[26] (108 cal/(mol Å^2) = 76 dyn/cm), which we anticipate is close to that for SPC water, consistently underpredicts $G(r)$. The more accurate fit of $G(r)$ with a value of γ_∞ greater than the vapor−liquid interfacial tension of water reflects the suppression of water density fluctuations near the surface of a HS solute relative to the vapor−liquid interface.[27,28]

The contact water density can be used to calculate hydration free energies for these HS solutes, from which the surface tension or free energy/surface area coefficient as a function of solute size is obtained. From SPT,[8,29,30] the free energy of solvating a HS solute is defined in terms of $G(r)$ as follows,

$$\mu^* = \rho kT \int_0^R G(\lambda) 4\pi\lambda^2\,d\lambda \quad (2)$$

where R is the center-to-center distance of closest approach

(24) Berendsen, H. J. C.; Postma, J. P. M.; van Gunsteren, W. F.; Hermans, J. In *Intermolecular Forces: Proceedings of the Fourteenth Jerusalem Symposium on Quantum Chemistry and Biochemistry;* Pullman, B., Ed.; Reidel Publishing Co.: Dordrecht, The Netherlands, 1981; p 331.

(25) Jorgensen, W. L.; Madura, J. D.; Swenson, C. J. *J. Am. Chem. Soc.* **1984**, *106*, 6638.

(26) Alejandre, J.; Tildesley, D. J.; Chapela, G. A. *J. Chem. Phys.* **1995**, *102*, 4574.

(27) Weeks, J. D.; Selinger, R. L. B.; Broughton, J. Q. *Phys. Rev. Lett.* **1995**, *75*, 2694.

(28) Widom, B. In *Phase Transitions and Critical Phenomena*; Domb, C., Green, M. S., Eds., Academic Press: New York, 1972; Vol. 2, p 79.

(29) Reiss, H. Adv. *Chem. Phys.* **1965**, *9*, 1.

(30) Pierotti, R. A. *Chem. Rev.* **1976**, *76*, 717.

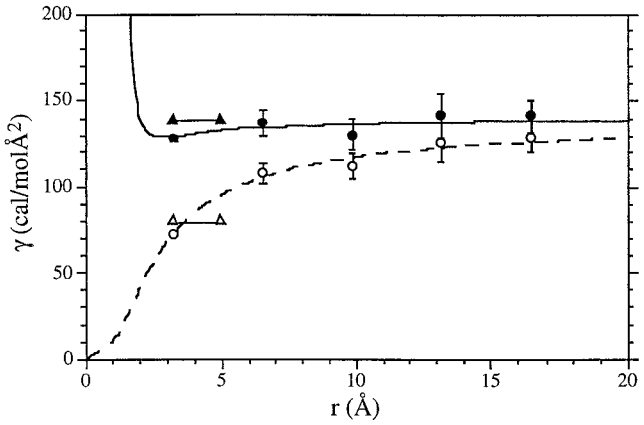

Figure 2. HS solute size dependence of the hydration free energy/surface area coefficient or surface tension defined with respect to the solvent-accessible (open circles) and van der Waals (filled circles) surfaces. Surface tensions derived from the simulations (open/filled circles) are compared to those calculated from eqs 3 and 4 (dashed and solid lines, respectively) using $G(r)$ obtained from eq 1 with $\gamma =$ 139 cal/(mol Å^2). The open and filled triangles represent corresponding values obtained from vacuum-to-water transfer free energies for cavity analogues of the *n*-alkane solutes, methane through *n*-hexane.[38] Simulation values of $G(r)$ are corrected for fluctuations in the simulation pressure and bulk density by subtracting $\ln(\rho^{sat}/\bar{\rho}_{corners})/\rho^{sat}kT\chi_T$, where $\bar{\rho}_{corners}$ is the average water density in the corners of the simulation box.

between the solute and a solvent molecule. Assuming pressure contributions are negligible, the molecular surface tension is obtained by taking the derivative of this expression with respect to solute surface area. The result depends, however, on the definition of the solute surface. Three widely used definitions are the van der Waals (vdW), molecular, and solvent-accessible (SAS) surfaces.[31−33] For spherical solutes, the vdW surface is equivalent to the molecular surface.[34] The SAS is defined as the surface traced by the center a sphere equivalent in size to a water molecule ($r_w = 1.4$ Å) as it is rolled over the vdW surface of the solute. The SAS of a spherical solute is $4\pi R^2$ and the surface tension is

$$\gamma_{SAS} = \rho kTRG(R)/2 \tag{3}$$

For the vdW or molecular surface, the surface area is $4\pi(R - r_w)^2$ and the surface tension is

$$\gamma_{vdW} = \rho kTR^2G(R)/2(R - r_w) \tag{4}$$

The calculated values of γ_{SAS} and γ_{vdW} are plotted as a function of solute size in Figure 2. On the basis of eqs 3 and 4, we expect γ_{SAS} and γ_{vdW} to be equivalent for large solutes but to diverge from one another as $R \rightarrow r_w$, which is the behavior observed in Figure 2. Surprisingly, γ_{vdW} is essentially constant and equal to $\gamma_\infty = 139$ cal/(mol Å^2) over the entire range of solute sizes considered. γ_{vdW} calculated using eq 1 accurately describes this behavior, but diverges as $R \rightarrow r_w$. This divergence occurs because a point solute with a vdW surface area of zero ($R = r_w$) has a nonzero water excluded volume of $4\pi r_w^3/3$ and a finite hydration free energy.[5] Nonetheless, for HS solutes the size of methane and larger, γ_{vdW} is essentially independent of solute size.

In contrast, γ_{SAS} varies considerably over the entire size range examined. This solute size dependence can be interpreted in the context of SPT as a curvature dependence of the surface tension.[8] Including only the leading term in this curvature dependence gives

$$\gamma_{SAS} \approx \gamma_\infty(1 - 2\delta/R) \tag{5}$$

where δ is the dewetting or Tolman length, which is a surface thermodynamic property of the water vapor−liquid interface (the distance between the equimolar surface and the surface of tension) and, as such, does not have a rigorous physical definition in the context of eq 5.[35] Here, we consider it to be an adjustable parameter of molecular size. Using eq 1 for γ_{SAS} and the fitted values of γ_∞ and G_2, we obtain $2\delta = 1.6$ Å. Moreover, from eqs 3 and 4,

$$\gamma_{vdW} = \gamma_{SAS}\frac{R}{R - r_w} \approx \gamma_\infty\left(\frac{R - 2\delta}{R - r_w}\right) \tag{6}$$

Since $r_w \sim 2\delta$, eq 6 predicts that γ_{vdW} is equal to γ_∞ over a wide range of solute sizes. In contrast, γ_{SAS} depends on solute size for $R \sim 2\delta$, as observed in Figure 2. These results will hold, however, only at temperatures near 25 °C, since the vapor−liquid interfacial tension of water decreases monotonically with increasing temperature, while the hydration free energies of methane-sized HS solutes exhibit a maximum with increasing temperature.[36] Thus, a nontrivial temperature dependence for δ is expected, as has been pointed out by others.[8,37]

Also shown in Figure 2 are the surface tensions obtained from a linear free energy/surface area correlation of vacuum-to-water transfer free energies of the cavity analogues of simple *n*-alkanes in SPC water.[38] In this case, the surface tension corresponding to the molecular surface is 138 cal/(mol Å^2), which is virtually identical to γ_∞ and hence γ_{vdW}. The agreement is striking given that these surface tensions are derived from entirely different thermodynamic processes—water density fluctuations in the present case and vacuum-to-water transfer or hydration free energies in the former. We note that differences in the surface tension have been reported in simulation studies of the hydration of a purely repulsive solute when it is deformed from a sphere (7 Å radius) into an oblate ellipsoid, indicating a solute shape dependence that was not examined in this work.[17] Surface tensions calculated for the repulsive LJ spherical solutes reported in that study are nonetheless comparable to those reported here.

Radial distribution functions for water oxygens around the methane clusters obtained from our simulations are plotted in Figure 3. $G(r)$ calculated using eq 1 with $\gamma_\infty = 139$ cal/(mol Å^2) is also shown in this figure. To compare these results with $G(r)$ for the HS solutes, we use the amplitude of the first peak in these cluster−water oxygen RDFs. Accordingly, we note that the first peak height in the cluster−water oxygen RDF decreases as the cluster size increases from a single methane to the 57-methane cluster. However, the first peak height for larger clusters is insensitive to the cluster size in contrast to $G(r)$ for the HS solutes. Moreover, unlike $G(r)$ for the HS solutes, the first peak heights for the cluster−water oxygen RDFs never

(31) Lee, B.; Richards, F. M. *J. Mol. Biol.* **1971**, *55*, 379.
(32) Richards, F. M. *Annu. Rev. Biophys. Bioeng.* **1977**, *6*, 151.
(33) Connolly, M. L. *Science* **1983**, *221*, 709.
(34) The molecular surface is defined as the locus of points tangent to a spherical water-sized probe when it is rolled over the vdW surface.
(35) Rowlinson, J. S.; Widom, B. *Molecular Theory of Capillarity*; Clarendon Press: Oxford, U.K., 1982; p 38.
(36) Garde, S.; Hummer, G.; García, A. E.; Paulaitis, M. E.; Pratt, L. R. *Phys. Rev. Lett.* **1996**, *77*, 4966.
(37) Huang, D. M.; Chandler, D. *Proc. Natl. Acad. Sci. U.S.A.* **2000**, *97*, 8324.
(38) Ashbaugh, H. S.; Kaler, E. W.; Paulaitis, M. E. *J. Am. Chem. Soc.* **1999**, *121*, 9243.

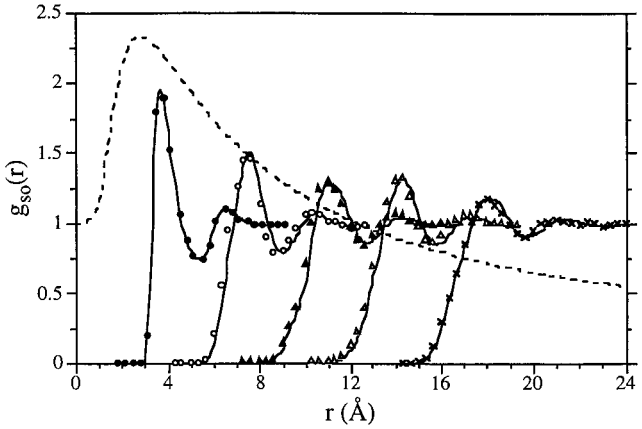

Figure 3. Methane cluster (center-of-mass)−SPC water oxygen RDFs for clusters of 1, 13, 57, 135, and 305 close-packed methane molecules. The symbols denote simulation values for clusters of 1(filled circles), 13 (open circles), 57 (filled triangles), 135 (open triangles), and 305 (crosses) methanes. The solid lines are RDFs predicted for each cluster based on the one-site proximity approximation (eq 7). The dashed line is $G(r)$ calculated using eq 1 with $\gamma = 139$ cal/(mol Å^2).

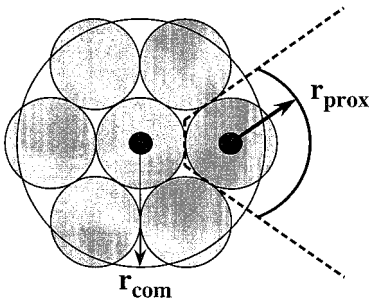

Figure 4. Schematic representation of a methane cluster in two dimensions showing, $\mathbf{r}_{com}$, the center-of-mass vector for a methane cluster and, $\mathbf{r}_{prox}$, the proximal vector for an individual methane molecule. The dashed lines denote the boundaries for determining water oxygens that are proximal to the methane molecule on the far right-hand side of the cluster.

drop below a value of 1, indicating that these larger methane clusters do not dewet to the extent observed for their HS analogues.

Insights into this dewetting behavior are obtained by calculating the local water structure around individual methanes in the different clusters, i.e., the methane−proximal water oxygen RDF for each cluster. This proximal distribution function is the number of water oxygens in a spherical shell of radius $\mathbf{r}_{prox}$ within the subdomain around each methane in a cluster, as shown in Figure 4. The subdomains are defined by a Voronoi tesselation of space with a node centered on each methane molecule. Proximal water densities within a subdomain are calculated as a function of radial distance from the methane center by averaging over the solid angle on a sphere defined by $\mathbf{r}_{prox}$ as shown in Figure 4.[39] The proximal RDFs for the methane clusters and for a single methane molecule are plotted in Figure 5. Although slight variations in first peak height are evident, the distribution functions are reasonably insensitive to the cluster size. We note that the converse also holds—i.e., the methane cluster−water oxygen RDFs in Figure 3 can be accurately described using only the methane−water oxygen RDF obtained from the simulations of a single methane in water.[39−41] The proximal distribution function description is based on the

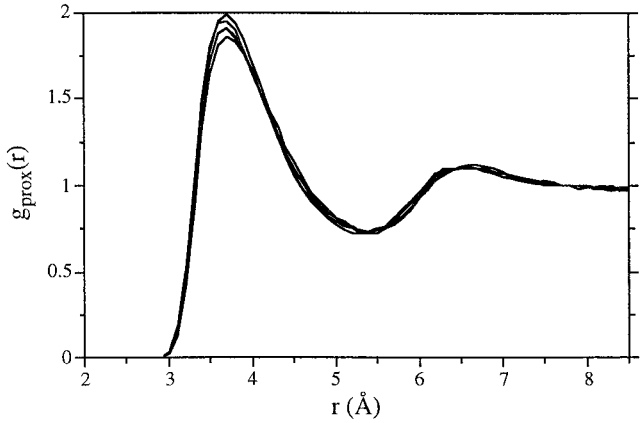

Figure 5. Methane−proximal water oxygen RDFs calculated from simulations for the individual clusters of 1, 13, 57, 135, and 305 close-packed methane molecules. No systematic variations in the height of the primary peak in these proximal RDFs were observed with cluster size.

assumption that water organization around a cluster is only locally sensitive to the structural details of that cluster. Thus, the conditional probability of finding a water molecule at $\mathbf{r}_w$ given that the N methane molecules in the cluster are located at ($\mathbf{r}_1$, ..., $\mathbf{r}_N$) is

$$\rho(\mathbf{r}_w|\mathbf{r}_1, ..., \mathbf{r}_N) \approx \rho g(|\mathbf{r}_w - \mathbf{r}_i|) \qquad (7)$$

with $|\mathbf{r}_w - \mathbf{r}_i| = \min_{j=1,...,N}|\mathbf{r}_w - \mathbf{r}_j|$ and where $g(|\mathbf{r}_w - \mathbf{r}_i|)$ is the methane−water oxygen RDF obtained from the simulations of a single methane in water.[21,22] The solid curves in Figure 3 are calculated by performing center-of-mass averaging of these local densities determined from eq 7. The good agreement observed in Figure 3 and the results in Figure 5 lead us to conclude that water organization around the individual methane molecules in the four methane clusters is essentially independent of the cluster size.

The effect of cluster size on the cluster−water oxygen RDF (Figure 3) can be attributed to two factors: the surface topology of the clusters and the collective effect of attractive interactions between each water molecule and the individual methane molecules in the cluster. Angle averaging over r_{com} in Figure 4 will attenuate spatial variations in the excluded-volume contribution to cluster−water interactions, effectively suppressing the water density in the first hydration shell of the cluster. Proximal water densities are not affected by these spatial variations since angle averaging over $\mathbf{r}_{prox}$ is performed locally around the individual, spherically symmetric elements of the cluster. Clearly, this effect of cluster surface topology will be most pronounced for the smaller clusters. The observed decrease in the first peak height of the cluster center-of-mass−water RDFs with increasing cluster size for the smaller clusters is, therefore, a manifestation this "roughness" of the cluster surface rather than intrinsic dewetting.

The higher water densities around the larger methane clusters relative to their HS analogues can be attributed to the collective effect of methane−water attractive interactions. We can examine the influence of these attractive interactions on the proximal RDF by applying the Weeks−Chandler−Anderson (WCA) decomposition of the methane−water LJ pair potential,[42]

(39) Ashbaugh, H. S.; Paulaitis, M. E. *J. Phys. Chem.* **1996**, *100*, 1900.
(40) Garde, S.; Hummer, G.; García, A. E.; Pratt, L. R.; Paulaitis, M. E. *Phys. Rev. E* **1996**, *53*, R4310.
(41) Ashbaugh, H. S.; Garde, S.; Hummer, G.; Kaler, E. W.; Paulaitis, M. E. *Biophys. J.* **1999**, *77*, 645.
(42) Weeks, J. D.; Chandler, D.; Anderson, H. C. *J. Chem. Phys.* **1971**, *54*, 5237.

$$\Phi_{MeO} = \Phi_{repulsive} + \lambda\Phi_{attractive} \tag{8a}$$

where

$$\Phi_{repulsive} = \begin{cases} 4\epsilon_{MeO}[(\sigma_{MeO}/r)^{12} - (\sigma_{MeO}/r)^{6}] + \epsilon_{MeO} & r < 2^{1/6}\sigma_{MeO} \\ 0 & r > 2^{1/6}\sigma_{MeO} \end{cases} \tag{8b}$$

$$\Phi_{attractive} = \begin{cases} -\epsilon_{MeO} & r < 2^{1/6}\sigma_{MeO} \\ 4\epsilon_{MeO}[(\sigma_{MeO}/r)^{12} - (\sigma_{MeO}/r)^{6}] & r > 2^{1/6}\sigma_{MeO} \end{cases} \tag{8c}$$

and σ_{MeO} and ϵ_{MeO} are the LJ diameter and well depth, respectively. The parameter λ interpolates between the purely repulsive ($\lambda = 0$) and the full ($\lambda = 1$) LJ potential. Values of λ greater than 1 correspond to even stronger attractions, i.e., LJ well depths greater than ϵ_{MeO}.

Methane−proximal water oxygen RDFs for the 57-methane cluster were calculated from simulations based on this pair potential function and values of λ between 0 and 2. The results are shown in Figure 6. For $\lambda = 0$, the first peak height in this proximal RDF is just slightly greater than $G(r)$ for the corresponding HS solute ($R = 9.85$ Å), while for $\lambda = 1$, this distribution function resembles the RDF for a single methane in water. Moreover, oscillations in the RDF become more pronounced with increasing λ, such that higher first peaks are obtained for larger values of λ. Clearly, enhanced methane−water attractive interactions produce higher proximal water densities, which in turn lead to higher water densities in the first hydration shell of the cluster as a whole. The collective nature of these attractive interactions is apparent when one considers that the first peak height in the methane−water oxygen RDF for a single methane in water is insensitive to methane−water attractive interactions (Figure 6 inset). We note that these results are reversible to changes in the attractive interactions; i.e., the wetting/dewetting transition does not appear to be an activated one. Starting from a representative, fully equilibrated water configuration around the attractive 57-methane cluster ($\lambda = 1$), water dewets this cluster when attractive interactions are turned off ($\lambda = 0$), and rewets the cluster when turned on again.

Liquid theories, such as WCA perturbation theory, take advantage of the fact that attractive forces in an isotropic fluid are weak and approximately sum to zero. Thus, liquid structure around a sufficiently small solute is determined largely by repulsive excluded-volume interactions. Near larger repulsive surfaces, however, the attractive forces in the fluid are unbalanced, and an additional effective repulsive potential—the effective cavity expulsion potential[20]—arises between the fluid and the surface due to the net attraction by the bulk fluid of solvent molecules near the surface. As a result, the fluid density near this surface is suppressed relative to the density for a purely repulsive fluid solvent with the same excluded volume (i.e., the fluid solvent without solvent−solvent attractive interactions). For the methane clusters studied here, the net methane−water attractive interactions compensate this expulsion potential, in effect, to rehydrate the cluster. The extent of rehydration is a monotonically increasing function of the strength of the methane−water attractive interaction (Figure 6). The quantitative agreement between the RDF for a single methane and the proximal RDFs in Figure 5 results from this balance between cavity expulsion and cluster attractive interactions.

Water hydrogen density distributions around the methane clusters and their HS analogues provides another comparison of hydration water structure. The HS solute−water hydrogen

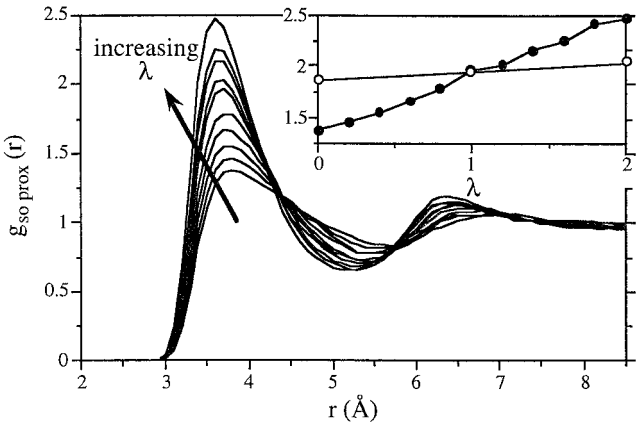

Figure 6. Methane−proximal water oxygen RDFs for the 57-methane cluster as a function of methane−water LJ attractive interactions (increasing λ) from purely repulsive interactions ($\lambda = 0$) to twice the LJ well depth ($\lambda = 2$). Inset: A comparison of the primary peak height in the proximal RDFs for the 57-methane cluster (filled circles) to those for a single methane molecule (open circles) over the range of LJ attractive interactions from $0 < \lambda < 2$.

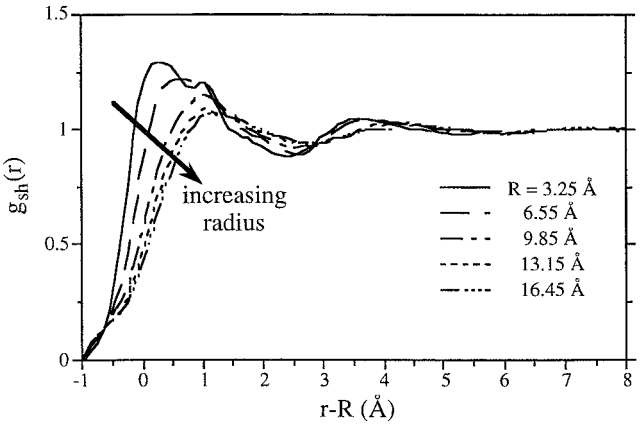

Figure 7. HS solute−SPC water hydrogen radial distribution functions for the HS radii indicated in the legend. To facilitate comparison, these RDFs are shifted to the left by the radius of the spherical excluded volume of SPC water oxygens.

RDFs obtained from simulation are plotted in Figure 7. For the methane-sized HS solute, the primary peak in this RDF has two maximums at ∼3.3 and ∼4.3 Å, which correspond to water molecules in the first hydration shell preferentially adopting orientations with their OH bond vectors pointing either radially outward from the solute (∼4.3 Å) or parallel to the solute surface (∼3.3 Å) in order to optimize water hydrogen bonding. These orientational preferences have been documented in numerous simulations and account for a significant portion of the unfavorable entropy of hydration at room temperature for simple, spherically symmetric nonpolar solutes.[43] This feature of the distribution function is, however, lost with increasing solute size, such that the maximum associated with hydrogen bonding parallel to the solute surface disappears, and the maximum associated with hydrogen bonding to water in the second hydration shell becomes the primary one, albeit suppressed relative to the methane-sized HS solute. These trends reflect the loss of water orientational structure in the first hydration shell and, as such, the decreasing impact of water orientational entropy on the free energy of hydration for the larger HS solutes. Indeed, we believe these observations account in part for the effect of solute size on the temperature dependence of γ.

The calculated methane−proximal water hydrogen RDFs for the clusters show similar behavior (Figure 8). For a single

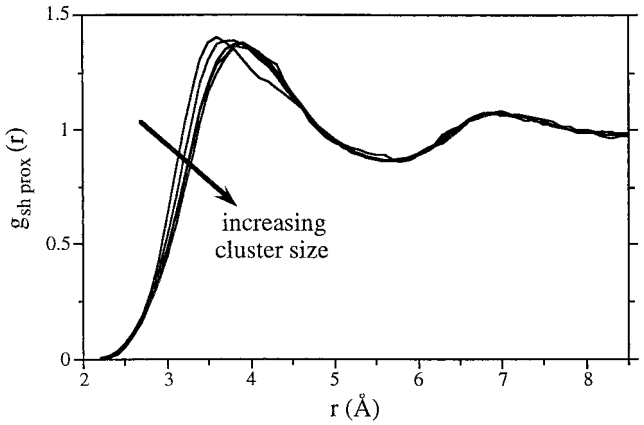

Figure 8. Methane−proximal water hydrogen RDFs calculated from simulations for the individual clusters of 1, 13, 57, 135, and 305 close-packed methane molecules. Increasing cluster size is indicated by the direction of the arrow.

methane in water, the primary peak in the distribution function has only one maximum. A shoulder on this peak is also evident, which reflects the same water orientational preferences noted above for the methane-sized HS solute. As the cluster size increases, the primary peak in the proximal RDF broadens, the shoulder disappears, and the peak maximum shifts to larger separations, indicating a breakdown in water structure in the first hydration shell around the individual methanes in the larger clusters.

Conclusions

The following observations have been made based on the results in Figure 2 for the HS solute size dependence of the surface tension. First, we obtain a surface tension of 139 cal/(mol Å^2) for the HS solutes, independent of solute size, when the surface tension is defined with respect to the van der Waals surface of the solute. This result applies to the hydration of HS solutes the size of methane (radius, 3.25 Å) and larger, including specifically HS solutes comparable in size to simple micelles or small globular proteins. Second, this value of the surface tension is virtually identical to that obtained in our previous simulation study of the hydration of a series of *n*-alkane-like cavities from methane through hexane.[38] The surface tension in that study was calculated from entirely different thermodynamic information: the slope of a linear correlation of vacuum-to-water transfer free energies plotted against solute molecular surface area, which is equivalent to the vdW surface for spherical solutes. Our previous study considered a wide range of *n*-alkane chain conformations from "completely folded" to extended; consequently, $\gamma = 139$ cal/(mol Å^2) independent of cavity shape for these simple *n*-alkane chains. The results in Figure 2 extend these previous findings to larger cavities and lead us to conclude that the free energy of cavity formation in water is simply proportional to the molecular surface area of the cavity,

$$\Delta G_{hyd} \propto \gamma A \tag{9}$$

with the proportionality constant or surface tension in this relationship equal to 139 cal/(mol Å^2) independent of cavity size for cavities the size of methane and larger. As noted above, $\gamma = 139$ cal/(mol Å^2) is somewhat greater than the macroscopic vapor−liquid interfacial tension of SPC/E water (108 cal/(mol Å^2)) obtained from molecular simulations of the vapor−liquid interface.[26] The discrepancy may be due in part to differences in water density fluctuations near the surface of a HS solute versus the free interface.[44] However, we cannot rule out the possibility that the surface tension depends on cavity size for cavities larger than those examined here, although we do not expect this to be the case.

Several observations have been made based on the results in Figure 2 for the surface tension defined with respect to the solvent-accessible surface. First, the macroscopic surface tension for the solvent-accessible surface asymptotically approaches 139 cal/(mol Å^2) with increasing HS solute radius, converging to γ_∞ obtained for the surface tension defined with respect to the van der Waals surface. Thus, γ_{vdW} and γ_{SAS} are equivalent in the limit of a macroscopic vapor−liquid interface, as predicted by eqs 5 and 6. In contrast to γ_{vdW}, however, γ_{SAS} decreases substantially with decreasing HS radius for radii less than ∼10 Å. Using the measured vapor−liquid interfacial tension of water (103 cal/(mol Å^2)), Chandler and co-workers[18] predicted similar behavior for γ_{SAS} based on a field theoretical model description of microscopic density fluctuations combined with a Gaussian description of local (molecular) density fluctuations in bulk water. They attributed the solute size dependence of γ_{SAS} for HS radii less than ∼4 Å to the Gaussian nature of water density fluctuations on these length scales, which is the basis of molecular theories of hydrophobicity, such as Pratt−Chandler theory,[45] as shown explicitly in the information theory model elaboration of SPT approaches to hydrophobic effects.[46,47] The behavior for larger HS radii is attributed to dewetting of the larger solute surfaces, which is qualitatively consistent with the radial distribution functions we obtained for the two largest HS solutes in Figure 1. The surprising result is that the surface tension defined with respect to the van der Waals surface is independent of solute size for HS solutes the size of methane and larger. For HS solutes smaller than methane, a diverging γ_{vdW} is clearly unphysical. However, from a practical point of view, nonpolar solutes smaller than methane are not relevant to a definition of the molecular surface tension quantified using *n*-alkane transfer free energies or to the application of this surface tension in eq 9 to describe hydrophobic driving forces that govern self-assembly in aqueous solution.

Clearly, solute−water attractive interactions play an important role in the wetting behavior of the larger solutes we studied. We find that water densities in the first hydration shell of the three largest methane clusters are both independent of cluster size and greater than bulk water density. In contrast, the water contact density for the HS analogues of these clusters decreases with solute size, falling below the density of bulk water for the two largest HS solutes. Thus, the large HS solutes dewet, while methane clusters of the same size do not. This dewetting is associated with a cavity expulsion potential, the impact of which increases with increasing solute size. The cavity expulsion potential arises due to water−water attractive interactions in the absence of concomitant solute−water attractive interactions. Conversely, the large methane clusters do not dewet because this cavity expulsion potential is offset by attractive interactions between the methane molecules that form the clusters and water molecules in the first hydration shell of these clusters. We do, however, observe a decrease in first hydration shell water densities for the smaller methane clusters with increasing cluster size. An analysis of proximal water distributions around the

(43) Lazaridis, T.; Paulaitis, M. E. *J. Phys. Chem.* **1992**, *96*, 3847 and references therein.
(44) Binder, K.; Müller, M. *Int. J. Mod. Phys. C* **2000**, *11*, 1093.
(45) Pratt, L. R.; Chandler, D. *J. Chem. Phys.* **1977**, *67*, 3683.
(46) Hummer, G.; Garde, S.; García, A. E.; Pohorille, A.; Pratt, L. R. *Proc. Natl. Acad. Sci. U.S.A.* **1996**, *93*, 8951.
(47) Hummer, G.; Garde, S.; García, A. E.; Paulaitis, M. E.; Pratt, L. R. *J. Phys. Chem.* **1998**, *102*, 10469.

individual methane molecules in all the clusters reveals that these distributions are independent of cluster size; i.e., all methanes are equally hydrated. We conclude, therefore, that this cluster size dependence for the smaller clusters is a manifestation of the molecular "roughness" of the cluster surface and not intrinsic dewetting.

The picture that emerges from these findings is stronger methane−water attractive interactions lead to higher proximal water densities around individual methane molecules regardless of cluster size. The higher proximal water densities, in turn, enhance preferential rewetting of the larger clusters relative to their purely repulsive HS analogues. The collective nature of these attractive interactions is clearly important and implies that the effect of solute−water attractive interactions on the hydration of the larger clusters cannot be accounted for by applying simple perturbation theories with the hard-sphere solute as the reference state. It is important to note that the balance between cavity expulsion and solute−water attractive interactions will also depend on the packing density of methane molecules in a cluster. A higher packing density would shift this balance to greater solute−water attractions and a more highly hydrated cluster. The packing density can also be changed by forming a polymer chain of methyl groups, and as such, the wetting/dewetting behavior will depend on the chain length as well as the chain conformation of polymeric solutes. The influence of chain packing on proximal water densities has been noted in previous simulation studies of the hydration of trans and gauche butane.[39] An understanding of the compensating effects of cavity expulsion and solute−water attractive interactions for topologically complex solutes ultimately will be required for a quantitative description of the hydrophobic driving forces governing self-assembly in aqueous solution.

Acknowledgment. We thank Shekhar Garde, Gerhard Hummer, and Lawrence Pratt for numerous fruitful discussions over the years. We are also indebted to Lawrence Pratt and Rohit Pappu for their careful reading of and insightful comments on the manuscript. Financial support from the National Science Foundation (CTS-0078491) is also gratefully acknowledged.

JA016324K